

Homoleptic Co(II), Ni(II), Cu(II), Zn(II) and Hg(II) complexes of bis-(phenyl)-diisoindol-aza-methene†

Roland Gresser,* Alexander Hoyer, Markus Hummert, Horst Hartmann, Karl Leo and Moritz Riede

Received 29th November 2010, Accepted 25th January 2011

DOI: 10.1039/c0dt01655a

The synthesis of five homoleptic transition metal complexes of bis-(phenyl)-diisoindol-aza-methene is described together with the optical, electrochemical and thermal properties of these compounds. Additionally, crystal structures for the Co and the Zn complex are reported.

Introduction

Dipyromethenes of the general structure **A** and their aza-methene analogue ligands **B** (Fig. 1) are able to form extremely stable complexes with a variety of metal or pseudo-metal ions, especially with boric acid derivatives yielding BODIPY and aza-BODIPY derivatives.^{1,2} This emerging material class has attracted enormous interest due to their intense absorption and strong fluorescence, especially in the red region of the spectrum. These outstanding properties stimulated the investigation of BODIPYs for various applications such as fluorescence probes for biological imaging,³ as emitter materials in organic light emitting diodes,⁴ or as absorber materials for organic solar cells.⁵

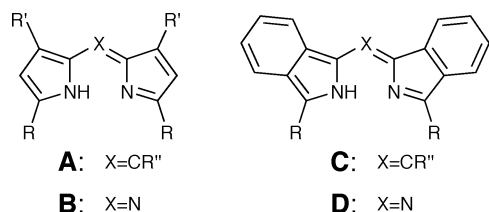


Fig. 1 Dipyromethenes, **A**, and their aza-methene analogues, **B**, and the corresponding (aza)-diisoindole-methenes, **C** and **D**.

In contrast to the chemistry of the boron containing BODIPYs and aza-BODIPYs, the chemistry of the metal complexes of (aza)-dipyromethenes, **A** (and **B**), developed significantly slower. However, in recent years, di- and tri-coordinative transition metal complexes of the compounds **A** and **B** were described. These complexes were prepared with a variety of metals like Ag(I), Au(I), Cu(I) and Co(II), Ni(II), Cu(II), Zn(II), and Hg(II), and their

structural and spectroscopic properties were investigated, in terms of supramolecular chemistry, light harvesting systems or metallic organic frameworks.⁶ To the best of our knowledge, in the case of bidentate metal complexes, with the (aza)-diisoindolemethene ligands, **C** (and **D**), only a copper compound was synthesized, but no spectroscopic data was given (Fig. 1).⁸ Recently, we reported a series of new aza-diisoindolemethene ligands, **D**, and the corresponding boron difluoride compounds.⁷ These complexes absorb, depending on their substituents, in the red or NIR (Near-infrared) region and the maximum can be related to an intense HOMO–LUMO transition. The more pronounced stabilization of the LUMO upon complexation with boron difluoride, originates in the bathochromic shift observed in the absorption spectra.⁷

In this study, we describe the synthesis and systematic characterization of five divalent transition metal derivatives of the aza-bis-(phenyl)-diisoindolemethene ligand,^{7–9} **D** (R = Ph, **1**), with Co(II), Ni(II), Cu(II), Zn(II), and Hg(II) as central metal ions, in order to support a better understanding of aza-BODIPY derivatives in the context of organic optoelectronics and enable the development of future applications.

For this purpose, the spectroscopic properties of these metal complexes were investigated and compared to the corresponding ligand and boron difluoride complex. Further quantum chemical calculations were performed to gain a deeper insight in the absorption properties, in particular into the absorption features of the Zn complex. The electrochemical behavior, which is dependant on the central metal ions, was determined by cyclic voltammetry. From single crystals of the Co and the Zn complexes, the molecular structure is revealed by X-ray diffraction and are presented and discussed. Since possible applications of these materials may occur by thermal evaporation in a vacuum, we also examined the thermal stability by thermogravimetric analysis in order to probe a potential processability.

Results and discussion

Synthesis

For the synthesis of the metal complexes, **2**, the corresponding metal(II)-acetate salts were reacted with two equivalents of **1** in either *n*-butanol or tetrahydrofuran (THF) as shown in Fig. 2.

Institut für Angewandte Photophysik, Fakultät für Physik, Technische Universität Dresden, George-Bähr-Strasse 1, 01069, Dresden, Germany. E-mail: roland.gresser@iapp.desxsxst; Fax: (+) 49-(0)351-463-37065

† Electronic supplementary information (ESI) available: Crystal structure and refinement data, thermogravimetric analysis of **1**, **3** and the Cartesian coordinates of the optimized structures **1** and **2d** together with additional molecular orbitals. CCDC reference numbers are 801539 (**2a**) and 801540 (**2d**). For ESI and crystallographic data in CIF or other electronic format see DOI: 10.1039/c0dt01655a

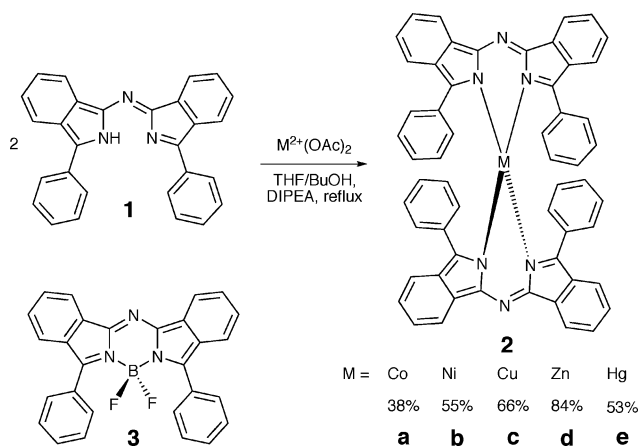


Fig. 2 Synthesis of the metal complexes, **2**.

This preparation method leads to the appropriate bis-homoleptic complexes, **2**, as crystalline solids in moderate to excellent yields, ranging from 38% to 84%. The Co, Ni, and Zn acetate salts were refluxed with the bis(phenyl)-aza-diisindole-methene ligand **1** in *n*-butanol, until no starting material could be assessed by thin layer chromatography (for **2a** and **2b**) or until the product precipitated (in the case of the Zn complex **2d**). The Cu and Hg complexes, **2c** and **2e**, were synthesized by heating the acetate salts in THF solution with diisopropylethylamine (DIPEA) for six hours for four days. In all cases, the precipitated products were purified by re-crystallization from dichloromethane/hexane solution, yielding pure crystalline complexes. The mass spectra of all prepared compounds, **2**, evidently showed the formation of the bis-homoleptic metal complexes **2a–2e**. As further characterization, ¹H NMR spectra were recorded for all compounds except for the paramagnetic Co and Cu complex, as might be expected. The Zn

and the Hg complexes typically gave spectra in the 0–10 ppm range. The ¹H NMR spectrum of the Ni complex is of particular interest, as it displayed considerable positive and negative peak shifts between –2 to +40 ppm at room temperature (see experimental section). Similar ¹H NMR characteristics were already described for a Ni bis-dipyrrromethene¹⁰ and other Ni complexes.¹¹ The distortion of the usually favored planar geometry to a pseudo-tetrahedral geometry due to the sterically demanding ligands in these complexes is given in the literature as an explanation and can also be expected to be the reason for **2b**. Nickel complexes exhibiting a pseudo-tetrahedral geometry, have short electron-spin lifetimes and therefore record well-resolved NMR spectra.¹⁰

Crystal structures

Single crystals of the Co and Zn complexes, **2a** and **2d**, were grown by slow evaporation of a chlorobenzene or toluene solution. Attempts to grow X-ray quality crystals for the other metal complexes, *e.g.* by slow vapor diffusion of pentane in a THF or chloroform solution, were not successful and resulted in crystals which were too small. Both the Co complex **2a** and the Zn complex **2d** crystallize in the triclinic space group $P\bar{1}$ with one solvent molecule in the unit cell (Fig. 3). Relevant interatomic distances and angles are summarized in Table 1. The molecular structure of both bis-chelates, **2a** and **2d**, can be regarded as a pseudo-tetrahedral coordination geometry with the metal atom in the center. The corresponding angle between the aza-diisindole planes are 68.0(6)° for the Co complex, **2a**, and 66.7(9)° for the Zn complex, **2d**, which is significantly distorted from an ideal D_{2d} symmetry, as shown in Fig. 3a and 3d. The metal–nitrogen bond lengths (M–N) range between 1.98(1) and 1.99(2) Å for the Co complex, **2a**, and are 1.99(1) and 1.99(8) Å long for the Zn complex, **2d**.

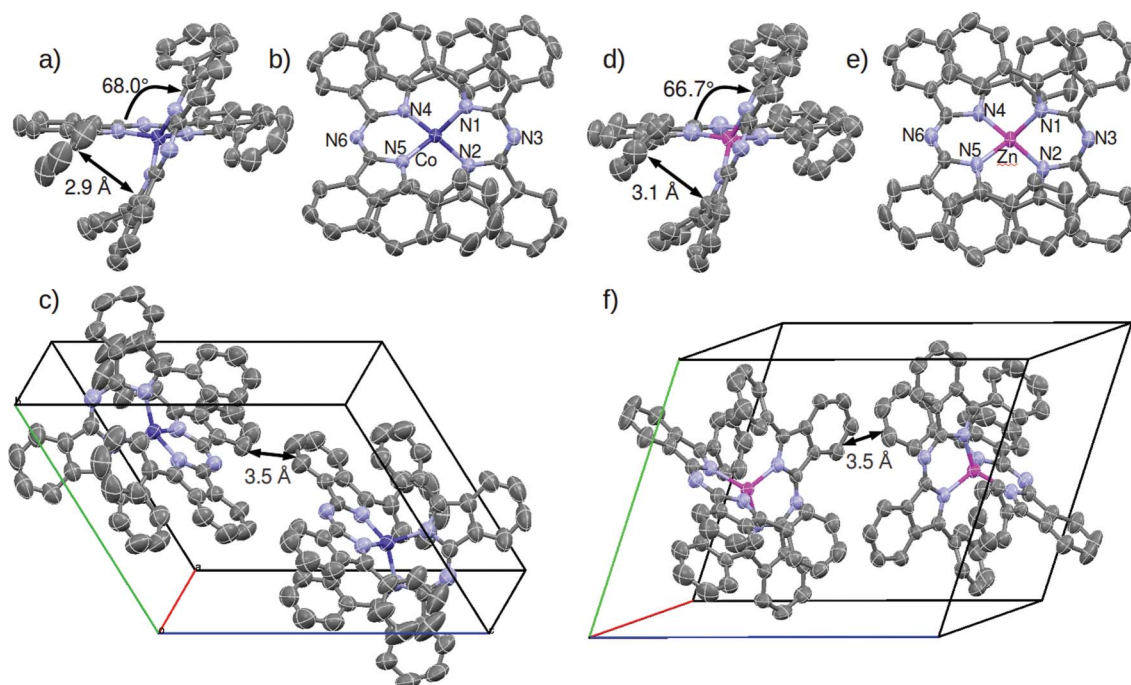


Fig. 3 Single crystal structure of the Co complex a–c and the Zn complex d–f. (a) and (d) Pseudo tetrahedral conformation; (b) and (e) top view; (c) and (f) unit cell (solvent molecule truncated for reasons of clarity). Hydrogen atoms are truncated in all cases for reasons of clarity as well.

Table 1 Selected bond lengths and angles obtained from the single crystal structure data

	2a (Co)	2e (Zn)
M–N1	1.99(1) Å	1.99(6) Å
M–N2	1.99(2) Å	1.99(3) Å
M–N4	1.98(1) Å	1.99(3) Å
M–N5	1.98(3) Å	1.99(8) Å
N1–M–N2	95.1(5) Å	94.2(2) Å
N4–M–N5	93.9(4) Å	95.3(4) Å
C–N3–C	126.2(4)°	128.0(4)°
C–N6–C	127.4(2)°	127.2(0)°
Plane angle	68.0(6)°	66.7(9)°

These bond lengths are similar to those found for comparable Zn(II) bis-dipyrromethene complexes,¹² but significantly longer than for the corresponding boron difluoride complex, with the N–B bond being 1.57(9) Å long.⁹

The nitrogen–metal–nitrogen (N–M–N) bite angle differs for each bis-isoindole aza-methene ligand in both metal complexes. In the Co complex, **2a**, the angle N1–Co–N2 is 95.15° and 93.94° for the N4–Co–N4 angle. In the Zn complex, **2d**, the angle is 94.2(2)° for the N1–Zn–N2 and 95.3(4)° for the N4–Zn–N4. The bite angle in the metal complexes is significantly smaller compared to the corresponding boron difluoride complex with 105.7(3)° and is consistent with the longer N–metal bond length. Additionally, the C–N3/6–C angle is widened in the metal aza-diisoindole bis-chelates in the range between 126.2(4)° and 128.0(4)° compared to 119.7(1)° in the boron difluoride complex.⁹ An interesting aspect is the sterically induced ligand–ligand interactions between the phenyl ring of one ligand and the aza-bis-isoindole plane of the opposite ligand, worthy of discussion in more detail. In the Co complex, **2a**, the minimum distance of the phenyl ring to the opposite isoindole plane is 2.9(0) Å, with an angle of 23.2(2)° to the plane. In the Zn complex, **2d**, the distance is slightly increased to 3.09(4) but the angle is decreased to 20.8(8). This distance of the phenyl ring to the isoindole plane in **2a** and **2d** is much shorter compared to non benzannulated aza-bodipy Zn complexes, having a minimum distance of 3.6(2) Å.¹² Therefore, an intermolecular π – π interaction can be considered to be present in these bis-chelate complexes. The interaction increases with an enlarging π -system. Accordingly, the distance of the phenyl ring plane to the opposite ligand is reduced in the benz-annulated aza-bis-isoindole-methenes compared to the aza-dipyrro-methenes with their smaller, non-annulated π -system on the backbone.¹²

Table 2 Absorption characteristics of the metal complexes, **2a–2e**, in comparison to **1** and **3**

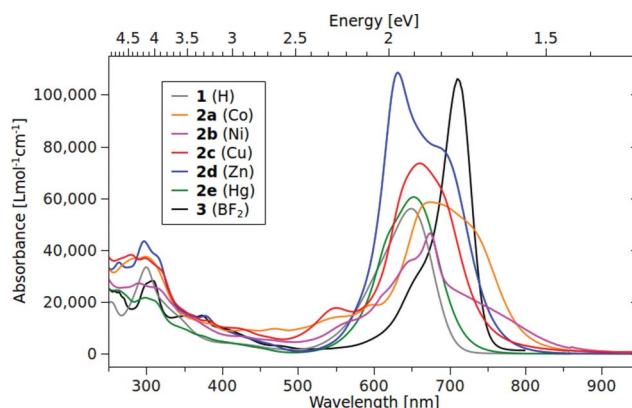
	λ_{UV}^a [nm]	Extinction [Lmol ⁻¹ cm ⁻¹]	λ_{max}^b [nm]	Extinction [Lmol ⁻¹ cm ⁻¹]	λ_{shou}^c [nm]	Extinction [Lmol ⁻¹ cm ⁻¹]
1 (H)	299	34 000	653	56 000	—	—
2a (Co)	298	37 500	674	58 500	725	50 500
2b (Ni)	288	27 000	674	46 500	645	35 500
2c (Cu)	290	38 000	656	73 500	—	—
2d (Zn)	297	43 000	632	108 500	685	80 500
2e (Hg)	260	24 000	653	60 500	626	49 500
3 (BF ₂)	305	28 000	715	106 000	—	—

Extinction coefficients are given for^a the most intense absorption in the UV region of the spectra, ^b the absorption maxima in the visible regime and ^c the most pronounced shoulder of the absorption maxima.

Absorption characteristics

The UV-Vis absorption properties of all the metal complexes **2a–2e** were investigated and compared with respect to the free ligand, **1**, and the boron difluoride complex, **3**, which were described elsewhere.^{7–9} The spectroscopic data are shown in Fig. 4 and are summarized in Table 2. All spectra of the ligand, **1**, and the metal complexes, **2a–2e**, exhibit an intense absorption band in the UV region, and an absorption maximum in the visible regime. In contrast to the spectrum of **1**, the absorption maxima of the metal complexes, **2a–2e**, display a broadening and the appearance of shoulders. The absorption maxima of the metal complexes are in the range between 632 nm and 674 nm in DCM, depending on the metal (Table 2). The Co and Ni complexes, **2a** and **2b**, show a red-shifted absorption maximum by 24 nm compared to the ligand, **1**, and an absorption tail extending into the NIR region over 800 nm. The absorption maximum of the Cu complex, **2c**, is red-shifted about 3 nm, with respect to the ligand, **1**, whereas the absorption maximum of the Hg complex, **2e**, is at the same wavelength. The Zn complex, **2d**, displays a hypsochromic shift of the maximum but exhibits an intense red-shifted shoulder at 685 nm, compared to **1**. All the metal complexes **2a–2e** feature, in comparison to the maximum, a strong absorbance in the UV part of the spectra around 300 nm as is also the case for the free ligand, **1**. This is in contrast to the boron difluoride complex, where this absorbance in the UV is weakened compared to the maximum.

The extinction coefficients of **2a–2e** are in the range of 46 000–108 000 Lmol⁻¹ cm⁻¹ for the corresponding absorption maxima and therefore increased compared to the ligand, **1**, except for the

**Fig. 4** Absorption spectra of the metal complexes, **2a–2e**, in dichloromethane. **1** and **3** are shown for comparison.

Ni complex, **2b** (Table 2). While the absorbance of the Co- and Ni complexes, **2a** and **2b**, is weak (with 46 500–58 500 Lmol⁻¹ cm⁻¹), the extinction increases from the Hg, **2e**, to the Cu, **2c**, and again to the Zn chelate, **2d**, from 60 500 to 73 500 and up to 108 500 Lmol⁻¹ cm⁻¹. This intense absorbance is comparable to the boron difluoride complex (as shown in our previous results)^{7,9} or even stronger in the case of the Zn complex, **2d**. The Zn complex, **2d**, displays the strongest absorbance for this ligand system so far.

All bis-(phenyl)-diisoindol-aza-methene metal complexes, **2a–2e**, are non-emissive and show no fluorescence, which is in contrast to **3**, since the boron difluoride compounds show an emission.⁹ Similar behavior was observed for (aza-dipyrromethene)-zinc(II) and -mercury(II) complexes,¹² but these aza-dipyrromethenes offer four rotatable phenyl-rings. However, since the more rigid compounds, **2**, do likewise not emit, the quenching is due to the heavy-atom effect, induced by the central transition metal ion.

Quantum chemical calculations

In order to study the absorption properties in more detail, the absorption spectra of the ligand, **1**, and the corresponding Zn complex, **2d**, regarded as a model system, were calculated with time-dependent density functional theory (TD-DFT, b3lyp/6-31g*).^{13,14} For this purpose, the geometries of both structures **1** and **2d** were optimized (ESI†) and the optical transitions up to the first ten excited states were calculated. Although the prediction of the absorption maximum deviated about 0.28 eV, the agreement with the observed spectra is good for **1** and **2d**, since both absorption features were predicted correctly.¹⁵ All absorption features in the aza-methene ligand system **1** result from a $\pi\text{-}\pi^*$ transition, as one might expect. The calculation of the absorption maximum in the visible regime for **1** clearly showed the principal orbital contribution for this absorption to be a HOMO→LUMO transition. In the ligand, **1**, the next occupied levels lower in energy (HOMO–1, –6.35 eV) and the next unoccupied levels higher in energy (LUMO+1, –0.89 eV) differ significantly in energy compared to the HOMO (–4.67 eV) and LUMO (–2.54 eV) energy values. Consequently, optical transitions from these lower lying occupied orbitals to the LUMO or LUMO+1 are involved for the high energy absorption in the UV (Table 3), in case of the ligand, **1**. The calculations on the optimized structure of the Zn complex, **2d**, showed degenerated HOMO energies (–4.56 eV) and nearly similar LUMO and LUMO+1 energies (–2.47 eV and –2.36 eV). This energetic situation, which is different to **1**, leads to several allowed optical transitions with absorption energies very close to each other, observed in the optical spectra as shoulders. The TD-DFT calculations revealed, that the absorption maximum including the shoulder in the visible region arises from two contributions. First, transitions from the HOMO→LUMO and HOMO–1→LUMO+1 lead to the most intense absorption. Secondly, the intense red-shifted shoulder arises due to transitions from the HOMO–1 to LUMO and the HOMO to LUMO+1. The relative intensities of these transitions were predicted in agreement with the experiment, with a lower extinction for the red-shifted shoulder in the case of the Zn complex, **2d**. For the high energy absorption in **2d**, detected in the UV region, deeper lying orbitals are involved, as for **1**, which are listed in detail in Table 3.

Calculations based on the single crystal structure of **2d** support the findings of the optimized structure. The results showed a

Table 3 Energy, oscillator strength and principal orbital contribution in the ligand, **1**, and the Zn complex, **2d**

	Energy [eV] (nm)	Oscillator strength	Principal orbital contributions
1	2.19 (567.21)	0.788	HOMO→LUMO
	3.14 (394.17)	0.016	HOMO→LUMO+1 HOMO–1→LUMO
	3.15 (392.80)	0.065	HOMO–2→LUMO HOMO→LUMO+1
2d^a	2.14 (577.16)	0.552	HOMO–1→LUMO HOMO→LUMO+1
	2.24 (553.26)	0.878	HOMO→LUMO HOMO–1→LUMO+1
	3.35 (369.48)	0.011	HOMO–4→LUMO+1 HOMO–3→LUMO HOMO–1→LUMO+4
	3.36 (368.92)	0.021	HOMO→LUMO+5 HOMO–4→LUMO HOMO–3→LUMO+1 HOMO–1→LUMO+5 HOMO→LUMO+4
	3.37 (366.88)	0.021	HOMO–4→LUMO HOMO–3→LUMO+1 HOMO–1→LUMO+5 HOMO→LUMO+4
2d^b	2.10 (588.63)	0.382	HOMO–1→LUMO HOMO→LUMO+1
	2.29 (540.12)	0.878	HOMO→LUMO HOMO–1→LUMO+1
	3.35 (369.48)	0.014	HOMO–4→LUMO+1 HOMO–3→LUMO HOMO–1→LUMO+4
	3.37 (366.88)	0.021	HOMO→LUMO+5 HOMO–4→LUMO HOMO–3→LUMO+1 HOMO–1→LUMO+5 HOMO→LUMO+4

Calculation with the optimized ligand structure, **1**,^a with the optimized Zn complex structure, **2d^a**, and ^b with the single crystal structure, **2d^b**.

quasi-degeneration of the HOMO and HOMO–1 energy levels with a deviation of only 0.0232 eV. This break-up of degeneracy compared to the optimized structure is most likely due to variations from an ideal D_2d symmetry, induced by solid state packing effects. However, the absorption features were predicted in the same way as for the optimized structure without any significant changes (Table 3). A detailed analysis of the frontier orbitals of the Zn complex, **2d**, (Fig. 5) displayed the HOMO and HOMO–1 orbital to be the only ligand located. The LUMO and LUMO+1 instead are partially metal located with a clearly visible alternation of the orientation of the metal d -orbital in the center. This indicates, that the optical transitions in **2d**, leading to the absorption maximum including the shoulder, have a partial ligand to metal $L(\pi)\text{-}M(d^*)$ charge transfer character (LMCT).

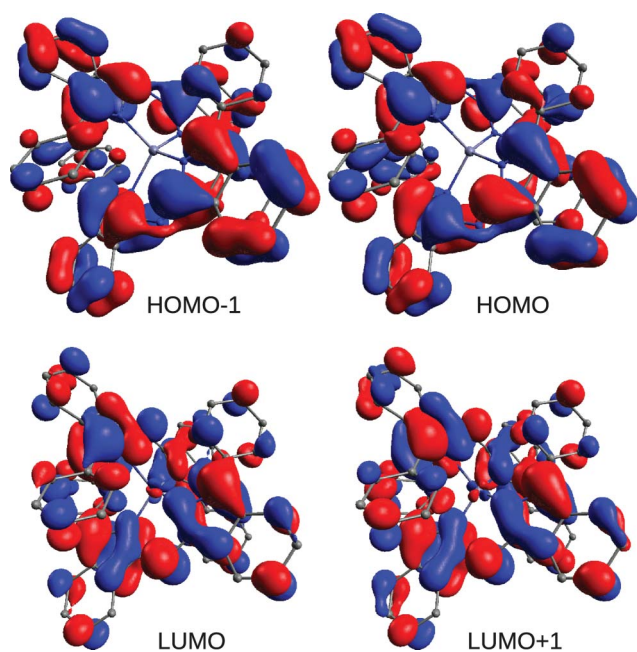
Electrochemical characterization

Since the redox potentials and the resultant HOMO and LUMO energies are important for (opto-)electronic applications, the electrochemical properties of all prepared complexes, **2a–2e**, were examined with cyclic voltammetry (CV), to obtain the corresponding oxidation and reduction potentials. The results were compared to the potentials of the free ligand, **1**, and the boron difluoride complex, **3**. The measurements were done in dichloromethane, using an Ag/AgCl reference electrode with the ferrocene/ferrocinium couple (Fc/Fc⁺) as the internal redox standard.¹⁶ The metal compounds, **2a–2e**, exhibit a complex electrochemical behavior. All reversible redox states were only

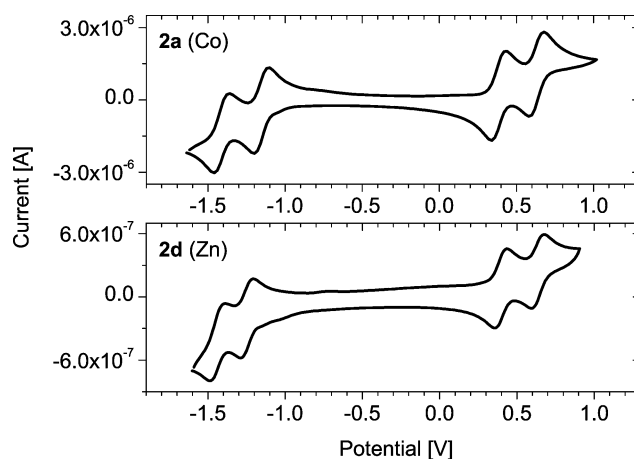
Table 4 Electrochemical data of the metal complexes, **2a–2e**, the ligand, **1**, and the boron difluoride complex, **3**, vs. Fc/Fc⁺

Compound	$E_{\frac{1}{2}}^{\text{red}2}$	$E_{\frac{1}{2}}^{\text{red}1}$	$E_{\frac{1}{2}}^{\text{ox}1}$	$E_{\frac{1}{2}}^{\text{ox}2}$
1 (H)	—	−1.44 ^a	0.18 ^a	—
2a (Co)	−1.78 ^a	−1.52 ^a	0.02 ^a	0.26 ^a
2b (Ni)	—	−1.36 ^b	−0.01 ^a	0.21 ^b
2c (Cu)	—	−0.78 ^b	−0.14 ^a	0.44 ^b
2d (Zn)	−1.78 ^a	−1.62 ^a	0.02 ^a	0.26 ^a
2e (Hg)	−1.59 ^b	−1.49 ^b	0.04 ^a	0.26 ^b
3 (BF ₂)	—	−1.12 ^a	0.43 ^a	—

Half wave potentials vs. Fc/Fc⁺ of the first reduction and oxidation and (if present) the second reduction and oxidation; measured in CH₂Cl₂/Bu₄PF₆ (0.1 M) vs. Ag/AgCl, scan rate 100 mV s^{−1}, with Fc/Fc⁺ as internal standard.^{17a} Reversible redox waves. ^b Irreversible redox waves.

**Fig. 5** Frontier orbitals of the optimized Zn complex, **2d**, involved in the lowest energy absorption. Note the ligand only character of the HOMO−1 and HOMO and the partial metal located LUMO and LUMO+1.

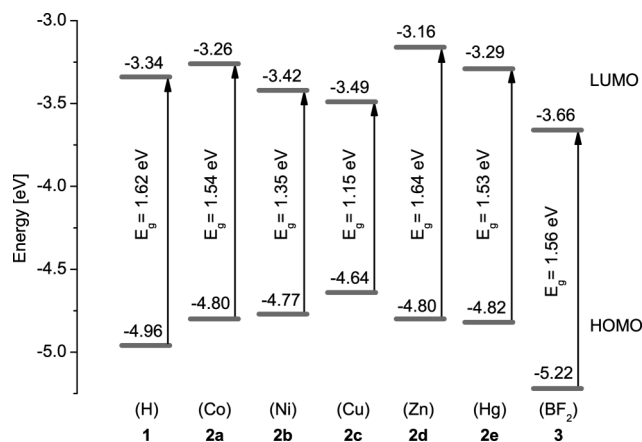
measured for the Co and Zn complexes, **2a** and **2d**, with two reversible oxidation and reduction waves (Fig. 5) in each case. The Co complex, **2a**, displayed potentials at −1.52 V vs. Fc and at −1.78 V vs. Fc for the first and the second reduction, respectively. The oxidation waves were observed at 0.02 V and 0.26 V vs. Fc for the first and second oxidation wave respectively (Fig. 6). The Zn complex, **2d**, showed the same redox potentials as the Co complex, **2a**, apart from the first reduction wave which was shifted by −100 mV to lower potentials. The complexes **2b** (Ni), **2c** (Cu) and **2e** (Hg) displayed only reversible one-electron oxidation waves, whereas the second oxidation and the one electron reduction (and two electron reduction for **2e**) processes appeared to be irreversible. All measured redox potentials are listed in Table 4. The one-electron reduction potentials of the Co, Ni, Cu, and Zn complexes, **2a–2d**, reflect the periodic trend of the electron affinity for the first row transition metal elements. In this trend one would expect an increase of the electron affinity from Co to Ni to Cu, and a decrease for Zn. The experimental reduction in fact becomes more facile from complex **2a** (Co) to **2b** (Ni) by 0.16 V, to **2c** (Cu) by 0.74 V, and

**Fig. 6** Reversible one- and two-electron redox waves for the Co and Zn complex, **2a** and **2d**, measured in CH₂Cl₂/Bu₄PF₆ (0.1 M) vs. Ag/AgCl, scan rate 100 mV s^{−1}, with Fc/Fc⁺ as internal standard.¹⁶

less favored for **2d** (Zn) by 0.10 V. This characteristic is represented in the LUMO energies in the Fig. 6.¹⁸

The one-electron oxidation shows a trend in the CV measurement with a decreasing ionization potential from complex **2a** (Co) to **2b** (Ni) by 0.03 V, to **2c** (Cu) by 0.16 V, and further increases in the potential for complex **2d** (Zn) and **2e** (Hg) by 0.02 V. On the one hand, this behavior is in contrast to the trend of the pure transition metals M(0), where a higher oxidation potential for Cu than for Co is expected, due to the higher ionization energy. On the other hand, this trend can be qualitatively understood with the simple Pearson's concept of hard and soft Lewis acid and bases (HSAB).¹⁹ In the HSAB concept, the hardness of transition metal ions (M²⁺) is decreasing (or the softness is increasing) in the periodic table by going from Co(II) via Ni(II) to Cu(II).²⁰ Consistently, the oxidation potentials of **2a–2c** are continuously shifted towards lower potentials. The higher oxidation potential of the Zn and the Hg compound, **2d** and **2e**, can be considered to be due to the additional stability of the electronic configuration for a closed *s*-atomic orbital shell.²⁰

The electrical gap of the metal complexes, **2a–2e**, obtained from the CV measurements (Fig. 7) does not correlate with the observed

**Fig. 7** Calculated HOMO and LUMO energy values from the obtained redox potentials; $E_{\text{HOMO}}(\text{Fc}) = -4.78$ eV, $E_{\text{HOMO}} = -4.78 + (E_{\frac{1}{2}}^{\text{ox}}(\text{Fc}) - (E_{\frac{1}{2}}^{\text{red}}))$, $E_{\text{LUMO}} = -4.78 + (E_{\frac{1}{2}}^{\text{ox}}(\text{Fc}) - (E_{\frac{1}{2}}^{\text{red}}))$.¹⁷

absorption properties (Fig. 4). According to the electrochemical data, the Cu complex, **2c**, should have the most red-shifted absorption, assuming a pure HOMO–LUMO transition. However, this is neither the case for the absorption maximum nor for the red-shifted shoulder occurring in the spectrum. For this reason, the electrochemical measurements confirm that no pure HOMO–LUMO transitions are present in the absorption process, as was evaluated by quantum chemical calculations for the Zn complex, **2d**.

Thermogravimetric analysis

To probe a possible processability of these materials by thermal vacuum sublimation, the thermal stability of the complexes, **2a–2e**, was investigated by differential thermal analysis (DTA) and thermogravimetric analysis (TGA).²¹ The mass loss of the metal complexes was measured by TGA in an inert nitrogen gas atmosphere, as shown in Fig. 8.

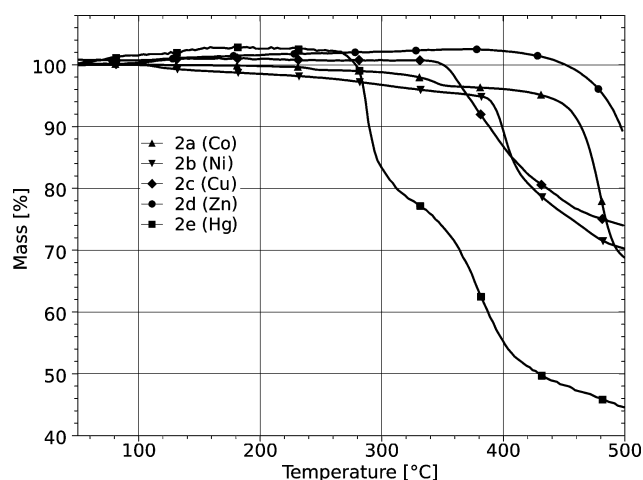


Fig. 8 Thermogravimetric analysis of the metal complexes, **2a–2e**, in the temperature regime of 50 to 500 °C.

Since the ligand, **1**, in these systems remained the same, the measured stability is related to the stability of the metal–nitrogen bond and the thermal activation of the metal(II)-ions and associated decomposition reactions. Although there is a mass drift present in a few samples, the decomposition proceeds very abruptly and hence allows for an objective analysis of the data. All of the investigated compounds, except the Hg complex, **2e**, exhibit a good thermal stability and a significantly increased stability compared to the free ligand, **1**.²¹ For compounds **2a–2d** incorporating first-row transition elements (Co, Ni, Cu and Zn), the thermal stability correlates with the oxidation potential of these complexes. The most stable compounds were those with Co and Zn as central metal atoms, **2a** and **2d**. These materials showed a negligible mass loss (<5%) until 420 °C but a rapid mass loss in higher temperature regimes. In terms of thermal stability, the next most stable compound is the Ni complex, **2b**, with a decomposition temperature around 385 °C, followed by the Cu complex, **2c**, with decomposition occurring at 345 °C. The Hg complex, **2e**, is the thermally most fragile compound with degradation occurring at 286 °C combined with a very rapid mass loss. This material behavior may be related to the larger Hg(II)-ion and hence a longer, and therefore weaker Hg–N bond, as was

shown for a related Hg complex.¹² It is worth mentioning, that the Co and the Zn complex, **2a** and **2d**, are both evaporable in a high vacuum (10^{-6} mbar) at moderate temperatures (~ 200 °C), offering an easy processability for further investigations.

Conclusions

The synthesis and systematic characterization of Co, Ni, Cu, Zn, and Hg complexes of aza-bis-(phenyl)-diisoidolmethene is described. The molecular structures of the Co and the Zn complexes, **2a** and **2d**, adopt a pseudotetrahedral geometry in the solid state, with a significant distortion from D_{2d} symmetry, as obtained from single crystal X-ray diffraction.

The absorption spectra of all complexes, **2a–2e**, are characterized by a broadening of the absorption maximum together with shoulders. The extinction coefficients are increased compared to the ligand, **1**, in particular for the Zn complex, **2d**, with the highest extinction for this ligand system so far. All complexes **2a–2e** are nonemissive. TD-DFT calculations of the Zn complex, **2d**, revealed that the absorption behavior originates from degenerate HOMO and HOMO–1 energies and transition from these orbitals into the LUMO and LUMO+1, with a partial ligand-to-metal charge transfer character. Cyclic voltammetry measurements showed a trend of decreasing oxidation and increasing reduction potential for the first-row transition metal complexes, **2a–2d**. This makes it possible to tune the electrochemical potential and hence the HOMO and LUMO energies simply by choosing the appropriate metal ion. Together with a good thermal stability (up to 460 °C for the Zn complex, **2d**) the metal complexes of the aza-bis-(phenyl)-diisoidolmethene offers a simple processability by thermal evaporation. Therefore, a further investigation for the application of these materials in organic solar cells is intended.

Experimental

All starting materials were obtained from commercial sources and were used without further purification. Tetrahydrofuran (THF) was dried over sodium and distilled right before use or stored over mole sieve 4 Å. Butanol was dried over mole sieves 4 Å. ¹H and ¹³C spectra were recorded at 25 °C with a Bruker DRX 500 P instrument at 500.13 and 125.76 MHz, respectively. The assignment of quaternary C, CH, CH₂ and CH₃ was completed using DEPT spectra. Elemental analysis achieved with an Eurovektor Hekatech EA-3000 elemental analyzer. The UV-VIS spectra were measured with a Perkin Elmer λ 25 spectrometer. Mass spectra were recorded with a Bruker Esquire-LC 00084 instrument, at 10 Volt with electrospray ionization with methanol (0.1% ammonium acetate). Melting points and DTA-TG were measured simultaneously with the thermal analyzer STA 409PC Luxx, direct mass spectroscopy were done with a capillary coupling to QMS 403 C Aëlos, both from NETZSCH.

Cyclic voltammetry was recorded with a Metrohm μ -Autolab potentiostat in a single-component cell under a nitrogen atmosphere. A typical three electrode configuration with an inlaid platinum disk as working electrode, platinum wire as counter electrode and a silver rod coated electrochemically with AgCl. Potentials were measured *versus* SCE and referenced to ferrocene as an internal standard ($E^\circ(\text{Fc}/\text{Fc}^+) = -4.78$ eV to vacuum). The measurements were performed with a scan rate of 100 mV s⁻¹ in

de-gassed dichloromethane (HPLC quality) and addition of tetra-*n*-butylammonium hexafluorophosphate (TBAPF, 0.1 mol L⁻¹) as electrolyte. Compound **1** was synthesized as described in ref. 7.

Cobalt-di-aza-bis-(phenyl)-diisoindolmethene (**2a**)

Compound **1** (1.00 g, 2.52 mmol) and 1.3 e.q. cobalt(II)-acetate (0.54 g, 3.09 mol) is refluxed *n*-butanol (20 mL) with 2 e.q. diisopropylethylamine (DIPEA) (0.7 mL, 4.95 mmol) until the product starts to precipitate from solution. The cold reaction mixture is filtered and the so obtained product is re-crystallized from dichloromethane/hexane (4:1), yielding the zinc-di-aza-bis-(phenyl)-diisoindolmethene as yellow needles (0.40 g, 37%), m.p. 383 °C, (dichloromethane/hexane 4:1). ¹H NMR: not possible. ¹³C NMR: not possible. ESI-MS *m/z* (%): [M+H]⁺ 852.3. Elemental analysis calcd. for C₅₆H₃₆N₆Co: C 78.96, H 4.26, N 9.87; found: C 78.84, H 4.17, N 9.75.

Nickel-di-aza-bis-(phenyl)-diisoindolmethene (**2b**)

Compound **1** (1.00 g, 2.52 mmol) and 1 e.q. nickel(II)-acetate (0.44 g, 2.52 mol) is refluxed *n*-butanol (20 mL) with 2 e.q. DIPEA (0.7 mL, 4.95 mmol) until the product starts to precipitate from solution. The cold reaction mixture is filtered and the so obtained product is re-crystallized from dichloromethane/hexane (4:1), yielding the zinc-di-aza-bis-(phenyl)-diisoindolmethene as yellow needles (0.58 g, 57%), m.p. 378 °C, (dichloromethane/hexane 4:1). ¹H NMR (500 MHz, CDCl₃): δ (ppm) = 40.55 (s, 4H), 13.75 (s, 2H), 6.71 (s, 2H), 6.42 (s, 4H), 5.49 (s, 2H), 3.93 (s, 2H), -1.96 (s, 2H); ¹³C: not possible due to low solubility. ESI-MS *m/z* (%): [M+H]⁺ 851.2. Elemental analysis calcd. for C₅₆H₃₆N₆Ni: C 78.98, H 4.26, N 9.87. Elemental analysis found: C 78.94, H 4.29, N 9.49.

Copper-di-aza-bis-(phenyl)-diisoindolmethene (**2c**)

Compound **1** (1.00 g, 2.52 mmol) and 1.3 e.q. copper(II)-acetate (1.08 g, 3.18 mmol) is refluxed THF (10 mL) with 3 e.q. DIPEA for 30 min. The solution is refluxed until no starting material is detectable with TLC. The reaction mixture is cooled to room temperature and the solid filtered. Re-crystallization from dichloromethane/hexane (4:1) gave the copper-di-aza-bis-(phenyl)-diisoindolmethene as violet plates (0.72 g, 66%), m.p. 344 °C, (dichloromethane/hexane 4:1). ¹H NMR: not possible. ¹³C NMR: not possible. ESI-MS *m/z* (%): [M+H]⁺ 856.3. Elemental analysis calcd. for C₅₆H₃₆N₆Cu: C 78.53, H 4.24, N 9.81; found: C 78.41, H 4.41, N 9.79.

Zinc-di-aza-bis-(phenyl)-diisoindolmethene (**2d**)

Compound **1** (1.00 g, 2.52 mmol) and 1.3 e.q. zinc(II)-acetate (0.60 g, 3.28 mol) is refluxed *n*-butanol (20 mL) with 2 e.q. diisopropylethylamine (DIPEA) (0.7 mL, 4.95 mmol) until the product starts to precipitate from solution. The cold reaction mixture is filtered and the so obtained product is re-crystallized from dichloromethane/hexane (4:1), yielding the zinc-di-aza-bis-(phenyl)-diisoindolmethene as yellow needles (0.91 g, 84%), m.p. 370 °C, (dichloromethane/hexane 4:1). ¹H NMR (500 MHz, CDCl₃): δ (ppm) = 8.07 (d, *J* = 7.88 Hz, 2H), 7.58 (d, *J* = 7.88 Hz, 2H), 7.40 (t, *J* = 7.88 Hz, 6H), 7.20 (t, *J* = 7.88 Hz, 2H), 6.93 (t,

J = 7.56 Hz, 4H), 6.83 (t, *J* = 7.56 Hz, 2H). ¹³C NMR (126 MHz, CDCl₃): δ (ppm) = 153.2, 141.5, 137.2, 132.8, 130.3, 128.6, 128.0, 127.4, 127.3, 124.9, 121.5, 120.6. ESI-MS *m/z* (%): [M+H]⁺ 857.3. Elemental analysis calcd. for C₅₆H₃₆N₆Zn: C 78.36, H 4.23, N 9.79; found: C 77.53, H 4.95, N 9.53.

Mercury-di-aza-bis-(phenyl)-diisoindolmethene (**2e**)

Compound **1** (1.00 g, 2.52 mmol) and 1.3 e.q. mercury(II)-acetate (1.08 g, 3.41 mmol) is refluxed THF (10 mL) with 3 e.q. DIPEA for 30 min. The solution is refluxed until no starting material is detectable with TLC. The reaction mixture is cooled to room temperature and the solid filtered. Re-crystallization from dichloromethane/hexane (4:1) gave the copper-di-aza-bis-(phenyl)-diisoindolmethene as violet plates (0.66 g, 53%), m.p. 286 °C, (dichloromethane/hexane 4:1). ¹H NMR (500 MHz, CDCl₃): δ (ppm) = 8.10 (d, *J* = 7.92 Hz, 2H), 7.59 (d, *J* = 7.90 Hz, 2H), 7.45 (t, *J* = 7.98 Hz, *J* = 7.04 Hz, 2H), 7.42 (d, *J* = 7.92 Hz, 4H), 7.26 (t, *J* = 6.99 Hz, 2H), 6.98 (m, 6H). ¹³C NMR (126 MHz, CDCl₃): δ (ppm) = 153.8, 140.9, 137.8, 133.6, 130.2, 129.0, 128.4, 127.3, 124.8, 121.5, 120.5. ESI-MS *m/z* (%): [M+H]⁺ 993.3. Elemental analysis calcd. for C₅₆H₃₆N₆Hg: C 67.70, H 3.65, N 8.46; found: C 67.24, H 3.36, N 8.92.

Acknowledgements

The authors gratefully acknowledge the financial support by the Federal Ministry for Education and Research (BMBF) within the Innoprofile program (03IP602) and the computational resources from the Center for Information Services and High Performance Computing (ZIH), TU Dresden. For the thermal analysis, the authors would like to thank Prof. Dr Peer Schmidt and Hannelore Dallmann.

Notes and references

- (a) R. Ziessel, G. Ullrich and A. Harriman, *New J. Chem.*, 2007, **31**, 496–501; (b) A. Loudet and K. Burgess, *Chem. Rev.*, 2007, **107**, 4891–4932; (c) T. E. Wood and A. Thompson, *Chem. Rev.*, 2007, **107**, 1831–1861.
- (a) F. Bergstrom, I. Mikhalyo and P. Hagglof *et al.*, *J. Am. Chem. Soc.*, 2002, **124**(2), 196–204; (b) S. Diring, F. Puntoriero and F. Nastasi *et al.*, *J. Am. Chem. Soc.*, 2009, **131**(17), 6108; (c) A. Harriman, L. J. Mallon and K. J. Elliot *et al.*, *J. Am. Chem. Soc.*, 2009, **131**(37), 13375–13386.
- A. Hepp, G. Ulrich, R. Schmechel, H. von Seggern and R. Ziessel, *Synth. Met.*, 2004, **146**(1), 11–15.
- (a) T. Rousseau, A. Cravino, T. Bura, G. Ulrich, R. Ziessel and J. Roncal, *Chem. Commun.*, 2009, 1673–1675; (b) T. Rousseau, A. Cravino and T. Bura *et al.*, *J. Mater. Chem.*, 2009, **19**(16), 2298–2300.
- (a) T. P. Ivanov and A. Draganov, *Mh. Chem.*, 1968, **99**, 1990–2003; (b) JP 11092479.
- (a) S. R. Halper and S. M. Cohen, *Inorg. Chem.*, 2005, **44**, 486; (b) S. R. Halper, L. Do, J. R. Stork and S. M. Cohen, *J. Am. Chem. Soc.*, 2006, **128**, 15255; (c) L. Yu, K. Muthukumar, I. V. Sazanovich, C. Kirmaier, E. Hindin, J. R. Diers, P. D. Boyle, D. F. Bocian, D. Holten and J. S. Lindsey, *Inorg. Chem.*, 2003, **42**, 6629.
- R. Gresser, M. Hummert, H. Hartmann, K. Leo and M. Riede, *Chem. Eur. J.*, DOI: 10.1002/chem.201002941.
- H. Bredereck and H. W. Vollmann, *Chem. Ber.*, 1972, **105**, 2271–2283.
- V. F. Donyagina, S. Shimizu, N. Kobayashi and E. A. Lukyanets, *Tetrahedron Lett.*, 2008, **49**, 6152–6154.
- A. Palma, J. F. Gallagher, H. Müller-Bunz, J. Wolowska, E. J. L. McInnes and D. F. O'Shea, *Dalton Trans.*, 2009, 273–279.
- (a) E. Szajna, P. Dobrowolski, A. L. Fuller, A. M. Arif and L. M. Berreau, *Inorg. Chem.*, 2004, **43**, 3988; (b) L. Do, S. R. Halper and S. M. Cohen, *Chem. Commun.*, 2004, 2662; (c) L. Yu, K. Muthukumar, I. V. Sazanovich, C. Kirmaier, E. Hindin, J. R. Diers, P. D. Boyle,

- D. F. Bocian, D. Holten and J. S. Lindsey, *Inorg. Chem.*, 2003, **42**, 6629.
- 12 Thomas S. Teets, David V. Partyka, James B. Updegraff III and Thomas G. Gray, *Inorg. Chem.*, 2008, **47**, 2338–2346.
- 13 The TD-DFT approach has proven to be superior compared to semi-empirical methods; see J. Fabian, *Dyes Pigm.*, 2010, **84**(1), 36–53.
- 14 (a) *Gaussian 03, Revision E.01*, M. J. Frisch, G. W. Trucks, H. B. Schlegel, G. E. Scuseria, M. A. Robb, J. R. Cheeseman, J. A. Montgomery Jr., T. Vreven, K. N. Kudin, J. C. Burant, J. M. Millam, S. S. Iyengar, J. Tomasi, V. Barone, B. Mennucci, M. Cossi, G. Scalmani, N. Rega, G. A. Petersson, H. Nakatsuji, M. Hada, M. Ehara, K. Toyota, R. Fukuda, J. Hasegawa, M. Ishida, T. Nakajima, Y. Honda, O. Kitao, H. Nakai, M. Klene, X. Li, J. E. Knox, H. P. Hratchian, J. B. Cross, V. Bakken, C. Adamo, J. Jaramillo, R. Gomperts, R. E. Stratmann, O. Yazyev, A. J. Austin, R. Cammi, C. Pomelli, J. W. Ochterski, P. Y. Ayala, K. Morokuma, G. A. Voth, P. Salvador, J. J. Dannenberg, V. G. Zakrzewski, S. Dapprich, A. D. Daniels, M. C. Strain, O. Farkas, D. K. Malick, A. D. Rabuck, K. Raghavachari, J. B. Foresman, J. V. Ortiz, Q. Cui, A. G. Baboul, S. Clifford, J. Cioslowski, B. B. Stefanov, G. Liu, A. Liashenko, P. Piskorz, I. Komaromi, R. L. Martin, D. J. Fox, T. Keith, M. A. Al-Laham, C. Y. Peng, A. Nanayakkara, M. Challacombe, P. M. W. Gill, B. Johnson, W. Chen, M. W. Wong, C. Gonzalez, and J. A. Pople, Gaussian Inc., Wallingford CT, 2004;
- (b) See the ESI,† for computational details, cartesian coordinates of the optimized structures, and frontier orbital visualizations for **1**.
- 15 In order to obtain the most accurate results, benchmark calculations were performed according to M. Bühl and H. Kabrede, *J. Chem. Theory Comput.*, 2006, **2**, 1282–1290. It turned out that the b3lyp functional gave the best results for the prediction of the absorption energies compared to the bp86, pbe and the tpss functionals which gave deviations of over 0.6 eV.
- 16 J. Heinze, *Angew. Chem.*, 1984, **96**, 823–840.
- 17 By using the half wave oxidation and reduction potentials of the compounds, **2a–e**, the HOMO and LUMO energies have been calculated with the potential of Fc/Fc⁺ as reference energy of $E_{\text{HOMO}} = -4.78$ eV from N. G. Connelly and W. E. Geigerm, *Chem. Rev.*, 1996, **96**, 877–910.
- 18 (a) A. F. Holleman, N. Wiberg, in *Lehrbuch der Anorganischen Chemie*, de Gruyter, Berlin, 1995, vol. **101**, pp. 1202–1204; (b) A. F. Holleman, N. Wiberg, in *Lehrbuch der Anorganischen Chemie*, de Gruyter, Berlin, 1995, vol. **101**, pp. XXXVIII.
- 19 (a) R. G. Pearson, *J. Am. Chem. Soc.*, 1963, **85**(22), 3533–3539; (b) R. G. Pearson, *J. Chem. Educ.*, 1968, **45**, 581–586; (c) R. G. Pearson, *J. Chem. Educ.*, 1968, **45**, 643–648.
- 20 A. F. Holleman, N. Wiberg, in *Lehrbuch der Anorganischen Chemie*, de Gruyter, Berlin, 1995, vol. **101**, p. 1213.
- 21 A comparison of the thermal stability in the lower temperature regime between the Hg complex, the free ligand and the corresponding boron difluoride compound can be found in the ESI†.